Suplemento de la Revista Mexicana de Física **3** 0308091 (2022) 1–5

Longitudinal dynamics in light-front holographic QCD and hadron spectroscopy

Chandan Mondal

Institute of Modern Physics, Chinese Academy of Sciences, Lanzhou 730000, China,
School of Nuclear Science and Technology, University of Chinese Academy of Sciences, Beijing 100049, China

Received 11 January 2022; accepted 18 April 2022

We demonstrate that the 't Hooft equation and the light-front holographic Schrödinger equation are complementary to each other in governing the longitudinal and the transverse dynamics of color confinement in mesons (quark-antiquark) and baryons (quark-diquark). Together, they describe remarkably well the spectroscopic data for the light-light, heavy-light and heavy-heavy hadrons. In all hadrons, the transverse dynamics of confinement is controlled by the universal emerging hadronic scale of the light-front holography, $\kappa \sim 0.5$ GeV, which, in heavy-heavy hadrons, coincides with the 't Hooft coupling that governs the longitudinal confinement. This reflects the restoration of the rotational symmetry in the non-relativistic limit.

Keywords: Light-front holographic QCD; 't Hooft equation; confinement; hadron spectroscopy.

DOI: https://doi.org/10.31349/SuplRevMexFis.3.0308091

1. Introduction

The bound state problem of two-particle systems in $(3+1)$-dimension light-front QCD is cast into the following eigenvalue equation [1]

$$M^2 = \int \mathrm{d}x\mathrm{d}^2\mathbf{b}_\perp \Psi^*(x,\mathbf{b}_\perp) \left[-\frac{\nabla^2_{b_\perp}}{x(1-x)} + \frac{m_q^2}{x} + \frac{m_{\bar{q}}^2}{1-x}\right] \times \Psi(x,\mathbf{b}_\perp) + \text{interactions}\,, \quad (1)$$

where $\Psi(x,\mathbf{b}_\perp)$ is the light-front wave function (LFWF) of the system with x and $\mathbf{b}_\perp$ being the light-front momentum fraction carried by the quark and the transverse distance between the quark and the spectator, respectively. The system mass is denoted by M, whereas m_q and $m_{\bar{q}}$ are the effective masses of the quark and the antiquark (diquark) in the meson (baryon). Meanwhile, the '*interactions*' refer to an effective confining potential.

Introducing the light-front variable $\boldsymbol{\zeta} = \sqrt{x(1-x)}\mathbf{b}_\perp$, the wave function can be factorized into a transverse mode $\phi(\zeta)$ and a longitudinal mode $X(x)$,

$$\Psi(x,\zeta,\varphi) = \frac{\phi(\zeta)}{\sqrt{2\pi\zeta}} e^{iL\varphi} X(x)\,, \quad (2)$$

where $L = |L_z^{\max}|$ is the light-front orbital angular momentum and $X(x) = \sqrt{x(1-x)}\chi(x)$. While the exact derivation of the confining potential from first principle remains an open question, we assume that the transverse and the longitudinal confining potentials, $U_\perp(\zeta)$ and $U_\parallel(x)$, respectively, are independent to each other. The effective confining potential is then written as

$$U(x,\zeta) = U_\perp(\zeta) + U_\parallel(x)\,. \quad (3)$$

Under this approximation, Eq. (1) can be rewritten as

$$M^2 = M_\perp^2 + M_\parallel^2\,, \quad (4)$$

where

$$M_\perp^2 = \int \mathrm{d}^2\boldsymbol{\zeta}\phi^*(\zeta)\left[-\frac{d^2}{d\zeta^2} + \frac{4L^2-1}{4\zeta^2} + U_\perp(\zeta)\right]\phi(\zeta)\,, \quad (5)$$

and

$$M_\parallel^2 = \int \mathrm{d}x\chi^*(x)\left[\frac{m_q^2}{x} + \frac{m_{\bar{q}}^2}{1-x} + U_\parallel(x)\right]\chi(x)\,, \quad (6)$$

with the normalization conditions

$$\int \mathrm{d}x|\chi(x)|^2 = \int \mathrm{d}^2\boldsymbol{\zeta}|\phi(\zeta)|^2 = 1\,. \quad (7)$$

Being the confining potentials, $U_\perp(\zeta)$ and $U_\parallel(x)$ encode the complex dynamics of a QCD bound state.

2. Light-front holography and transverse confinement

Light-front holography neglects the longitudinal dynamics and considers the chiral limit, *i.e.*, massless quarks. The confining potential in transverse direction, *i.e.* $U_\perp(\zeta)$, is uniquely fixed by the underlying conformal symmetry and a holographic mapping to the anti-de Sitter $(\mathrm{AdS})_5$ [1–4]. This provides

$$U_\perp^{\mathrm{LFH}}(\zeta) = \kappa^4\zeta^2 + 2\kappa^2(J-1)\,, \quad (8)$$

where $J = L + S$ with S being the total quark-antiquark (diquark) spin and κ defines the strength of the confinement. The light-front variable ζ maps onto the fifth dimension of AdS_5. From Eq. (5), we can write

$$\left(-\frac{d^2}{d\zeta^2} + \frac{4L^2-1}{4\zeta^2} + U_\perp^{\mathrm{LFH}}(\zeta)\right)\phi(\zeta) = M_\perp^2\phi(\zeta)\,. \quad (9)$$

The above equation is identified as the wave equation for the freely propagating spin-J string modes in AdS_5.

In light-front holography, the longitudinal mode is not dynamical and it is fixed by mapping the pion electromagnetic or gravitational form factor in physical space-time, onto the one in AdS_5 [5, 6], which results in $\chi(x) = 1$, hence $X(x) = \sqrt{x(1-x)}$.

Solving the holographic Schrödinger equation, (9), for the mesons and baryons separately, as in Ref. [1], provides the meson mass spectrum as

$$M^2_{\perp,M} = 4\kappa^2 \left(n_\perp + L_M + \frac{S_M}{2} \right) \tag{10}$$

and the baryon mass spectrum as

$$M^2_{\perp,B} = 4\kappa^2 \left(n_\perp + L_B + \frac{S_D}{2} + 1 \right) , \tag{11}$$

where $n_\perp$ denotes the principal quantum number, S_M is the total quark-antiquark spin in the meson, and S_D is the diquark spin in the baryon. Note that Eq. (10) predicts that the lowest lying states with $n_\perp = L_M = S_M = 0$ are massless, as expected in the chiral limit.

3. The 't Hooft equation and longitudinal confinement

The longitudinal dynamics of a bound state can be described by the well known 't Hooft equation [7–10]. The Schrödinger-like equation derived by 't Hooft from the QCD Lagrangian in $(1+1)$-dimensions and in the large-N_c approximation is given by

$$\left(\frac{m_q^2}{x} + \frac{m_{\bar{q}}^2}{1-x} \right) \chi(x) + U_\parallel(x)\chi(x) = M^2_\parallel \chi(x) , \tag{12}$$

with

$$U_\parallel(x)\chi(x) = \frac{g^2}{\pi} \mathcal{P} \int \mathrm{d}y \frac{\chi(x) - \chi(y)}{(x-y)^2} , \tag{13}$$

where $g = g_s\sqrt{N_c}$ is the 't Hooft coupling with mass dimensions and $\mathcal{P}$ represents the principal value prescription. We use the 't Hooft equation for baryons by performing the transformation: $\bar{q}$ (antiquark) $\to [qq]$ (diquark).

Unlike the holographic Schrödinger equation, the 't Hooft equation does not have exact analytical solutions. To solve Eq. (12) numerically, we expand the longitudinal mode onto a Jacobi polynomial basis [8]

$$\chi(x) = \sum_n c_n f_n(x) , \tag{14}$$

with

$$f_n(x) = N_n x^{\beta_1}(1-x)^{\beta_2} P_n^{(2\beta_2, 2\beta_1)}(2x-1) , \tag{15}$$

where $P_n^{(2\beta_2,2\beta_1)}$ are the Jacobi polynomials and

$$N_n = \sqrt{(2n + 2\beta_1 + 2\beta_2 + 1)} \times \sqrt{\frac{n!\Gamma(n + 2\beta_1 + 2\beta_2 + 1)}{\Gamma(n + 2\beta_1 + 1)\Gamma(n + 2\beta_2 + 1)}} . \tag{16}$$

In this way, Eq. (12) takes the form of a matrix, which can then be diagonalized numerically. Note that our results are independent of the choice of basis, *i.e.* they remain stable with respect to variations in $\beta_{1,2}$.

The end-point analysis of the 't Hooft equation using the ansatz provided by the equation, that is the mode of the form [11]

$$\chi(x) \approx x^{\beta_1}(1-x)^{\beta_2} , \tag{17}$$

yields

$$\frac{\pi m_i^2}{g^2} - 1 + \pi\beta_i \cot(\pi\beta_i) = 0 . \tag{18}$$

In the chiral limit, the above equation provides

$$\beta_i = \sqrt{3m_i^2/\pi g^2} , \tag{19}$$

and

$$M_\pi^2 = g\sqrt{\frac{\pi}{3}}(m_u + m_d) + \mathcal{O}(m_u + m_d)^2 . \tag{20}$$

Despite the fact that the holographic Schrödinger equation, Eq. (9), predicts a massless pion, $M_\pi = 0$, the contribution to the pion mass is generated by the 't Hooft equation. Hence, together, the holographic Schrödinger equation and the 't Hooft equation predict the GMOR relation [12], which enclose the chiral symmetry breakng effects in QCD, $M_\pi^2 \propto m_{u/d}$.

The Heavy Quark Effective Theory (HQET) determines that the mass difference between the heavy-light vector and the pseudoscalar mesons in their ground states is suppressed by the heavy quark mass, $M^V_{Q\bar{q}} - M^P_{Q\bar{q}} \sim 1/m_Q$, while $M^{V/P}_{Q\bar{q}} \sim m_Q$. Together, the holographic Schrödinger equation and the 't Hooft equation also correctly predict the HQET constraint, when we presume that $\kappa(\ll m_Q)$ does not scale with m_Q [9, 10].

Meanwhile, the 't Hooft and the holographic potentials are consistent as they both correspond to an instant-form linear potential in the non-relativistic limit. Following the relation between light-front and instant-form potentials reported in Ref. [13], we have illustrated in Refs. [9, 10] that in the non-relativistic limit, both the longitudinal and the transverse light-front potentials are equivalent to instant-form linear potentials in the center-of-mass (CM) frame: $V_\parallel \sim (g^2/2)b_\parallel$ and $V_\perp \sim (\kappa^2/2)b_\perp$, respectively. Thus, with $g \sim \kappa$, the rotational symmetry is restored in the CM frame for the heavy-heavy system. In this context, an alternative longitudinal confining potential, $U_\parallel(x) = -\sigma^2\partial_x(x(1-x))\partial_x$, with σ being its longitudinal confinement scale, has been proposed in Ref. [14] and extensively used in literature [11, 15–23].

TABLE I. The quark masses and the longitudinal confinement scale, g, used to predict the hadron spectra. We use the transverse confinement scale $\kappa = 0.523 \pm 0.024$ GeV for all hadrons, and it coincides with g for hadrons with two heavy quarks.

Hadron	g [GeV]	$m_{u/d}$ [GeV]	m_s [GeV]	m_c [GeV]	m_b [GeV]
Light-light	0.128	0.046	0.357	—	—
Heavy-light	0.410	0.330	0.500	1.370	4.640
Heavy-heavy	0.523	—	—	1.370	4.640

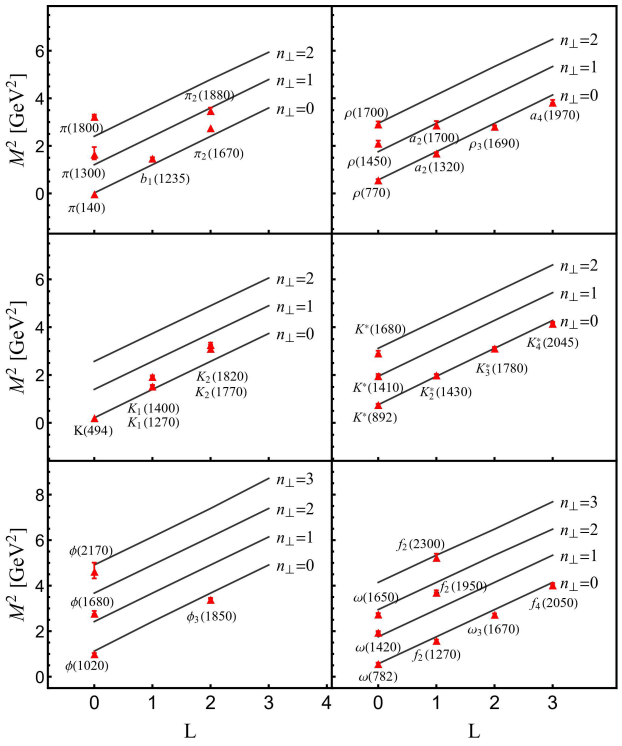

FIGURE 1. Regge slopes for the light-light meson states, compared with PDG data [24].

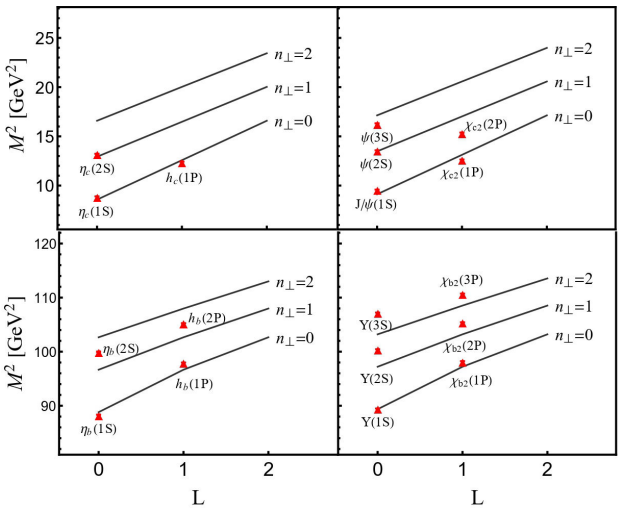

FIGURE 2. Regge slopes for the heavy-heavy meson states, compared with PDG data [24].

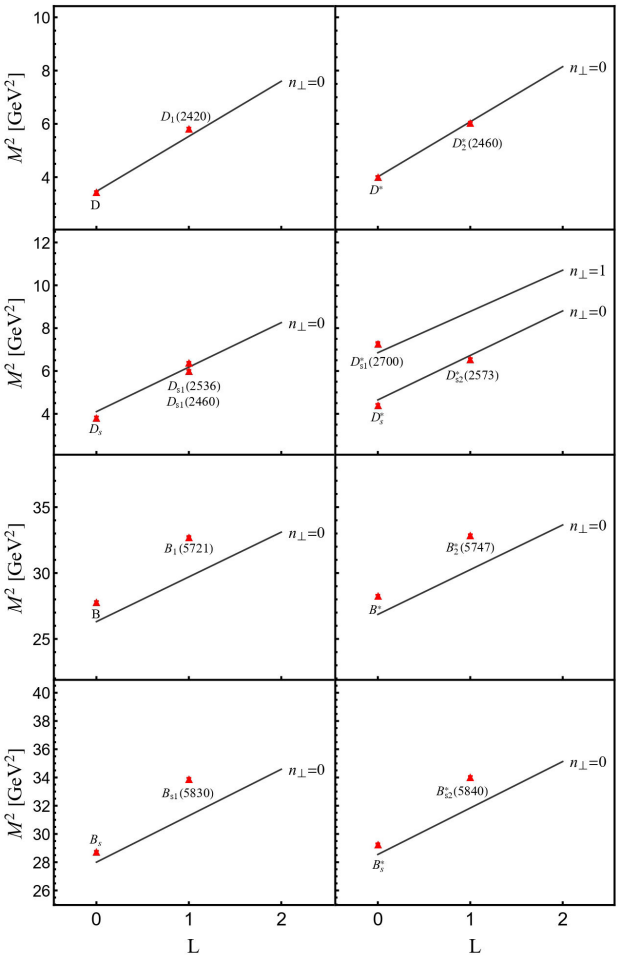

FIGURE 3. Regge slopes for the heavy-light meson states, compared with PDG data [24].

4. Results and Discussions

The total mass of the hadron states are evaluated using

$$M_M^2 = M_{\perp M}^2(n_\perp, L_M, S_M, \kappa) + M_{\parallel M}^2(n_\parallel, m_q, m_{\bar{q}}, g),$$
$$M_B^2 = M_{\perp B}^2(n_\perp, L_B, S_D, \kappa) + M_{\parallel M}^2(n_\parallel, m_q, m_{[qq]}, g). \quad (21)$$

Here, $n_\parallel$ is an additional (longitudinal) quantum number that emerges into the picture while solving the 't Hooft equation. The parity (P) and the charge conjugation (C) relations of the hadronic state are given by

$$P = (-1)^{L_M+1} = (-1)^{L_B}\ , \quad (22)$$

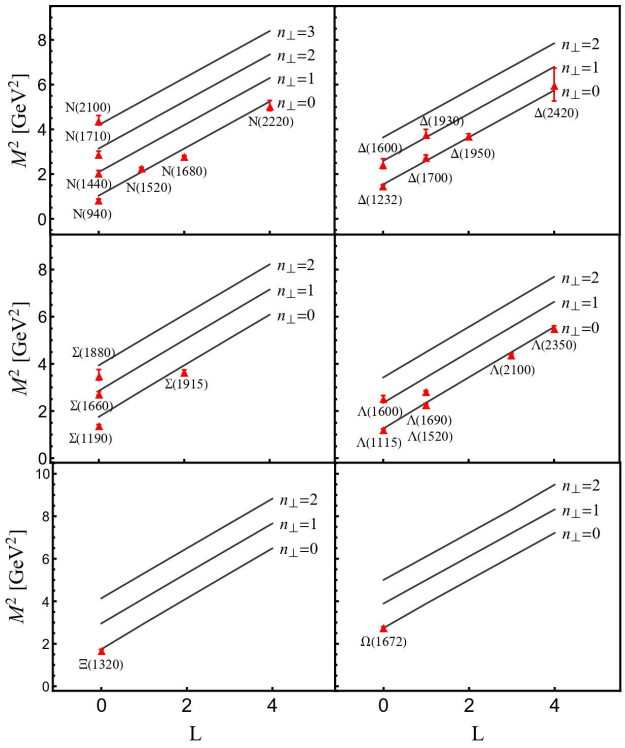

FIGURE 4. Regge slopes for the light-light baryon states, compared with PDG data [24].

and

$$C = (-1)^{n_\parallel + L_M + S_M}\,, \tag{23}$$

respectively. In addition, we find that an orbital and/or radial excitation in the transverse dynamics is always accompanied by an excitation in the longitudinal dynamics, *i.e.*,

$$n_\parallel \geq n_\perp + L\,. \tag{24}$$

To compute the hadron spectra, we adopt the quark masses and scale parameters as summarized in Table I and we consider the diquark mass to be the sum of the masses of the quarks in the diquark. Note that we use the universal κ, which is fixed to 0.523 ± 0.024 GeV [25] and vary g from light-light to heavy-light to heavy-heavy systems. In Figs. 1, 2, and 3 we show the Regge trajectories for all the meson states. For baryonic states, we present our numerical results in Figs. 4 and 5. Overall, we found a good agreement between our computed results for the hadron specta and the experimental data [24]. However, for the states containing one bottom quark (or antiquark) are less impressive, but the discrepancies lie below 10% in any case.

5. Conclusions

We have shown that the light-front holographic equation and the 't Hooft equation are complementary to each other in order to predict the hadron specta. While the holographic Schödinger equation produces the hadronic mass in the chiral limit of QCD with a universal emerging transverse confinement scale, the 't Hooft equation provides the contribution to the hadronic mass by taking into account the nonzero quark masses and the longitudinal confinement. Using these two equations, we have obtained a good quality description of the hadron specta comparing with the experimental data.

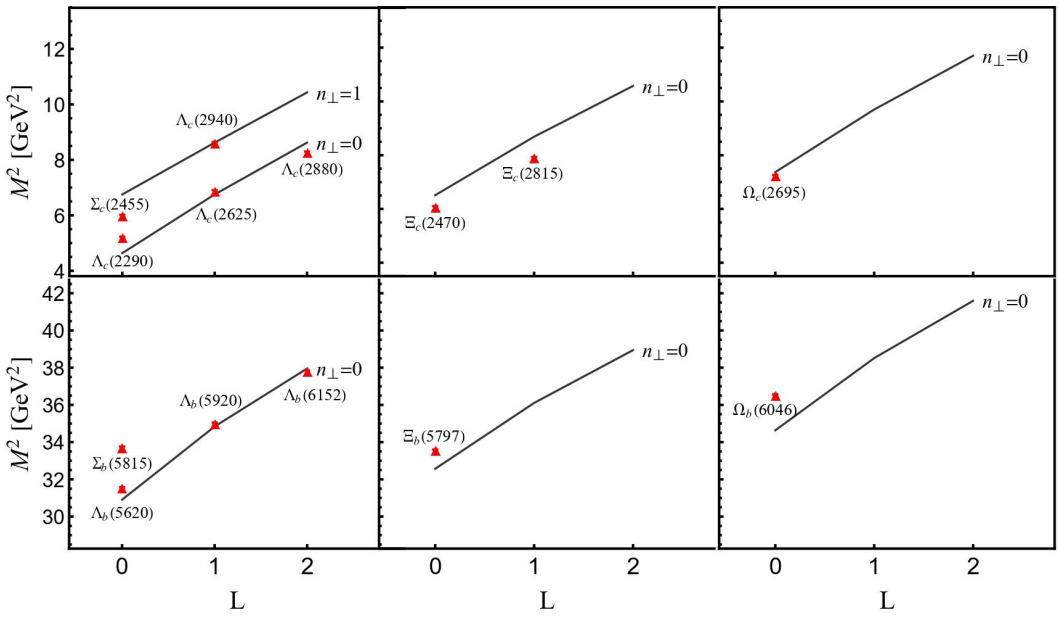

FIGURE 5. Regge slopes for the heavy-light baryon states, compared with PDG data [24].

Acknowledgement

I am grateful to Mohammad Ahmady, Harleen Dahiya, Satvir Kaur, Sugee Lee MacKay, Ruben Sandapen and Neetika Sharma for collaboration. I also thank Yang Li and Xingbo Zhao for many useful discussions. This work is supported by the Chinese Academy of Sciences Presidents International Fellowship Initiative, Grant No. 2021PM0023 and by new faculty start up funding by the Institute of Modern Physics, Chinese Academy of Sciences, Grant No. E129952YR0.

1. S. J. Brodsky, G. F. de Teramond, H. G. Dosch and J. Erlich, *Phys. Rept.* **584** (2015) 1-105, https://doi.org/10.1016/j.physrep.2015.05.001.
2. S. J. Brodsky and G. F. de Teramond, *Phys. Rev. Lett.* **96**, (2006) 201601, https://doi.org/10.1103/PhysRevLett.96.201601.
3. G. F. de Teramond and S. J. Brodsky, *Phys. Rev. Lett.* **94**, (2005) 201601, https://doi.org/10.1103/PhysRevLett.94.201601.
4. G. F. de Teramond and S. J. Brodsky, *Phys. Rev. Lett.* **102**, (2009) 081601, https://doi.org/10.1103/PhysRevLett.102.081601.
5. S. J. Brodsky and G. F. de Teramond, *Phys. Rev. D* **77**, (2008) 056007, https://doi.org/10.1103/PhysRevD.77.056007.
6. S. J. Brodsky and G. F. de Teramond, *Phys. Rev. D* **78**, (2008) 025032, https://doi.org/10.1103/PhysRevD.78.025032.
7. G. 't Hooft, *Nucl. Phys. B* **75**, (1974) 461-470, https://doi.org/10.1016/0550-3213(74)90088-1.
8. S. S. Chabysheva and J. R. Hiller, *Annals Phys.* **337**, (2013) 143-152, https://doi.org/10.1016/j.aop.2013.06.016.
9. M. Ahmady, H. Dahiya, S. Kaur, C. Mondal, R. Sandapen and N. Sharma, *Phys. Lett. B* **823**, (2021) 136754, https://doi.org/10.1016/j.physletb.2021.136754.
10. M. Ahmady, S. Kaur, S. L. MacKay, C. Mondal and R. Sandapen, *Phys. Rev. D* **104** (2021) 074013, https://doi.org/10.1103/PhysRevD.104.074013.
11. G. F. de Teramond and S. J. Brodsky, *Phys. Rev. D* **104** (2021) 116009, https://doi.org/10.1103/PhysRevD.104.116009.
12. M. Gell-Mann, R. J. Oakes and B. Renner, *Phys. Rev.* **175**, (1968) 2195-2199, https://doi.org/10.1103/PhysRev.175.2195.
13. A. P. Trawiński, S. D. Głazek, S. J. Brodsky, G. F. de Téramond and H. G. Dosch, *Phys. Rev. D* **90** (2014) 074017, https://doi.org/10.1103/PhysRevD.90.074017.
14. Y. Li, P. Maris, X. Zhao and J. P. Vary, *Phys. Lett. B* **758**, (2016) 118-124, https://doi.org/10.1016/j.physletb.2016.04.065.
15. Y. Li and J. P. Vary, *Phys. Lett. B* **825**, (2022) 136860, https://doi.org/10.1016/j.physletb.2021.136860.
16. A. B. Sheckler and G. A. Miller, *Phys. Rev. D* **103** (2021) 096018, https://doi.org/10.1103/PhysRevD.103.096018.
17. C. M. Weller and G. A. Miller, *Phys. Rev. D* **105** (2022) 036009, https://doi.org/10.1103/PhysRevD.105.036009.
18. J. Lan, C. Mondal, S. Jia, X. Zhao and J. P. Vary, *Phys. Rev. Lett.* **122** (2019) 172001, https://doi.org/10.1103/PhysRevLett.122.172001.
19. J. Lan, C. Mondal, S. Jia, X. Zhao and J. P. Vary, *Phys. Rev. D* **101** (2020) 034024, https://doi.org/10.1103/PhysRevD.101.034024.
20. J. Lan, C. Mondal, M. Li, Y. Li, S. Tang, X. Zhao and J. P. Vary, *Phys. Rev. D* **102** (2020) 014020, https://doi.org/10.1103/PhysRevD.102.014020.
21. C. Mondal, S. Xu, J. Lan, X. Zhao, Y. Li, D. Chakrabarti and J. P. Vary, *Phys. Rev. D* **102** (2020) 016008, https://doi.org/10.1103/PhysRevD.102.016008.
22. S. Xu *et al.* [BLFQ], *Phys. Rev. D* **104** (2021) 094036, https://doi.org/10.1103/PhysRevD.104.094036.
23. J. Lan *et al.* [BLFQ], *Phys. Lett. B* **825** (2022) 136890, https://doi.org/10.1016/j.physletb.2022.136890.
24. P. A. Zyla *et al.* [Particle Data Group], *PTEP* **2020** (2020) 083C01, https://doi.org/10.1093/ptep/ptaa104.
25. S. J. Brodsky, G. F. de Téramond, H. G. Dosch and C. Lorcé, *Int. J. Mod. Phys. A* **31** (2016) 1630029, https://doi.org/10.1142/S0217751X16300295. [arXiv:1606.04638 [hep-ph]].